Monatshefte für Chemie - Chemical Monthly (2019) 150:1841–1847
https://doi.org/10.1007/s00706-019-02471-x

ORIGINAL PAPER

Molybdic acid immobilized on mesoporous MCM-41 coated on nano-Fe_3O_4: preparation, characterization, and its application for the synthesis of polysubstituted coumarins

Hamideh Mohamadi Tanuraghaj[1] · **Mahnaz Farahi**[1]

Received: 4 May 2018 / Accepted: 24 June 2019 / Published online: 13 August 2019

Abstract

In this study, Fe_3O_4@MCM-41-$(CH_2)_3$-$OMoO_3H$ as a new recyclable nanocatalyst was synthesized and characterized by FT-IR, X-ray diffraction patterns, transmission electron microscopy, energy-dispersive X-ray spectroscopy, and vibrating sample magnetometer analysis. The performance ability of this novel magnetic heterogeneous catalyst was evaluated for the synthesis of coumarin derivatives by the one-pot reaction between aryl aldehydes, benzamide, and 5,7-dihydroxycoumarins. Fe_3O_4@MCM-41-$(CH_2)_3$-$OMoO_3H$ is a nontoxic and recoverable catalyst that provides an environmentally friendly reaction condition. This catalyst can be stored for a long times without a significant loss in its activity.

Graphic abstract

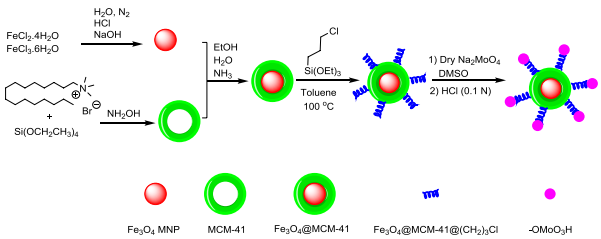

Keywords MCM-41 · Nano-Fe_3O_4 · Nanostructures · Heterogeneous catalysis · Aldehydes · 5,7-Dihydroxycoumarins · Benzamide

Introduction

In recent decades, mesoporous silica materials have been subjected to numerous investigations, due to their applications in many fields such as biotechnology [1], biomedicine [2], optical imaging [3], and catalysis [4]. The great number of advantages such as the tunable structural parameters (pore size, pore volume, and surface area), high surface area, and particularly sufficient silanol groups for surface modification has led to the emerging of this important class of materials as a promising catalyst [5]. Flexible modification regimes with nanocrystals of other inorganic materials are proposed to expand their practical uses in the area of heterogeneous catalytic systems [6–8].

Nanoscopic materials have received a major interest in particular, magnetic nanoparticles (MNPs) which have brought out some new kind of catalysts [9–11]. In this sense, a lot of attention has been focused on Fe_3O_4 magnetic nanoparticles thanks to their supermagnetism, high concavity, low Curie temperature, and nontoxicity [12–14]. Pure Fe_3O_4 nanoparticles tend to be oxidation in an air atmosphere and aggregation. Therefore, in the absence of any proper surface coating, they become stuck together, forming large clusters, resulting in limited functional groups and losing the specific properties. Therefore, a proper protection strategy has been

✉ Mahnaz Farahi
farahimb@yahoo.com; farahimb@yu.ac.ir

[1] Department of Chemistry, Yasouj University, P. O. Box 353, Yasouj 75918-74831, Iran

employed to stabilize bare iron oxide nanoparticles over long periods chemically [15].

The core–shell composite nanostructures consisting of an Fe_3O_4 magnetic nanoparticles core and a mesoporous silica shell with great potential in catalytic applications integrate the magnetic properties of Fe_3O_4 MNPs with the features of mesoporous materials [16–18]. Subsequently, it can greatly improve the performance of the catalyst and even generate new synergetic properties [19, 20]. Its surface modification can manipulate the mesoporous silica shell with silanol groups, which can conjugate with a range of different chemical entities [21]. The unique compatibility and consistency between these nanocatalysts and green chemistry are due to the faster and more practical separation methods by the use of an external magnet without any filtration that reduces solvent consumption, so that it can be a savior for environmental and energy challenges. The other noticeable features of these porous magnetic nanocatalysts can refer to chemically stability, low toxicity, being affordable, and high potency and activity [22–27].

To the best of our knowledge, coumarin and its derivatives constitute one of the major classes of naturally occurring compounds. A wide variety of biological activities such as anti-HIV [28], anti-oxidant [29], antifungal [30], anthelmintic [31], and antibacterial properties [32] have been reported for these compounds. Furthermore, they have found applications in optical [33], food [34], and cosmetic industries [35]. Coumarin derivatives also occupy an important position in organic synthesis ascribed to their key role in the preparation of pharmacologically active heterocyclic compounds [36]. Accordingly, much effort has been focused towards the development of versatile and efficient procedures for the preparation of coumarins [37, 38]. However, some of these methods suffer from at least one of the following drawbacks: long reaction time, difficult working conditions, tedious work-up procedures, and low yields [39].

Herein, in continuation of our studies in the field of heterogeneous catalysts [40–42] and according to the importance of coumarins, we wish to present the preparation and characterization of novel immobilized molybdic acid onto Fe_3O_4@MCM-41 nanoparticles [Fe_3O_4@MCM-41-$(CH_2)_3$-$OMoO_3H$] as well as studying its catalytic application in the synthesis of coumarin derivatives.

Results and discussion

The new magnetic nanocatalyst Fe_3O_4@MCM-41-$(CH_2)_3$-$OMoO_3H$ was prepared according to the protocol shown in Scheme 1. The core–shell structure was obtained by coating of a layer of prepared MCM-41 on the synthesized Fe_3O_4 core. Then, the surface of MCM-41 was functionalized by (3-chloropropyl)trimethoxysilan molecule. Finally, chloride group replaced by molybdic acid and the desired magnetic nanocatalyst was prepared. Chemical analysis of prepared Fe_3O_4@MCM-41-$(CH_2)_3$-$OMoO_3H$ was performed using FT-IR, energy-dispersive X-ray spectroscopy (EDX), X-ray diffraction (XRD), and transmission electron microscopy (TEM).

Figure 1 shows XRD patterns of MCM-41 (a) and Fe_3O_4@MCM-41-$(CH_2)_3$-$OMoO_3H$ (b) in low angle (0.7–10). The characteristic peaks of MCM-41 are seen around 2θ of 2.4°, 4.7°, and 5.5°, attributed to the (100), (110), and (200) reflections, confirming the highly ordered and hexagonal mesoporous structure of MCM-41 [43]. In the low angle XRD pattern of Fe_3O_4@MCM-41-$(CH_2)_3$-$OMoO_3H$ (Fig. 2), the intensity of the main peak was decreased and its width was increased, and both peaks at

Scheme 1

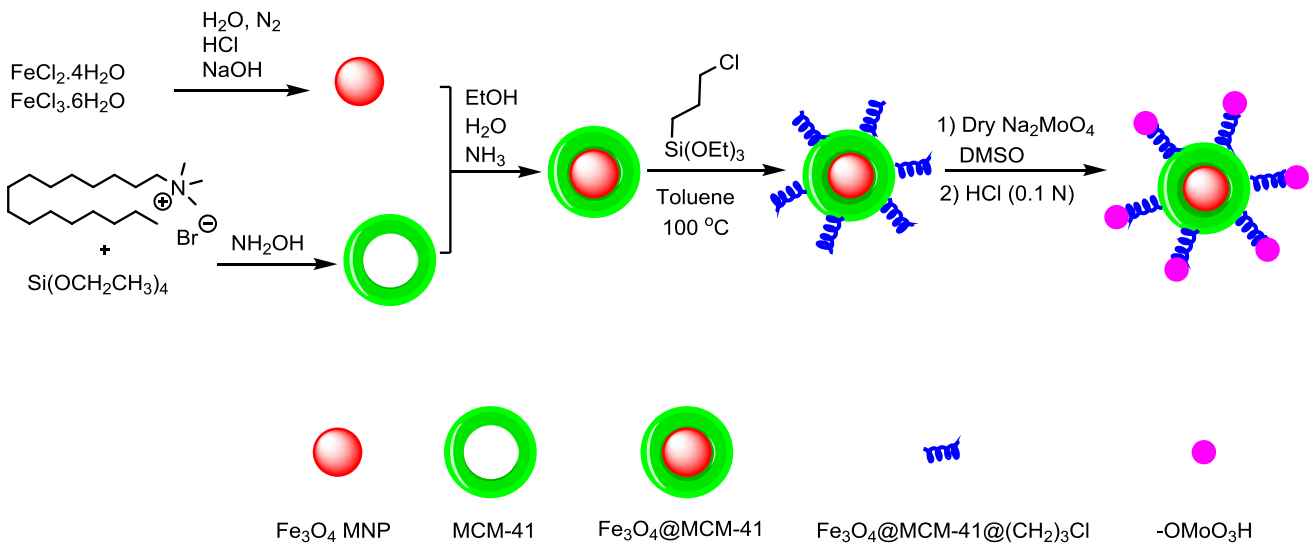

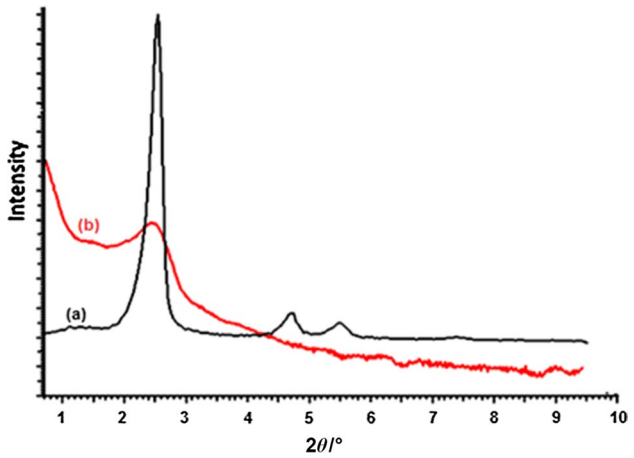

Fig. 1 Low angle XRD patterns of (a) MCM-41 and (b) Fe_3O_4@MCM-41-$(CH_2)_3$-$OMoO_3H$

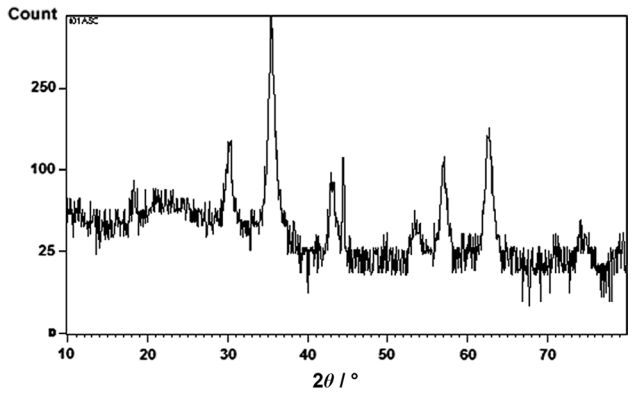

Fig. 2 Wide angle XRD patterns of Fe_3O_4@MCM-41-$(CH_2)_3$-$OMoO_3H$

$2\theta = 4.7°$ and 5.5° disappeared. These observations indicate that Fe_3O_4@MCM-41-$(CH_2)_3$-$OMoO_3H$ still has a hexagonal mesoporous structure but with less order, which might be ascribed to the location of Fe_3O_4 inside the lattice of MCM-41. Wide angle XRD patterns of Fe_3O_4@MCM-41-$(CH_2)_3$-$OMoO_3H$ exhibit six strong diffraction peaks at $2\theta = 29.5°$, 36.2°, 43.7°, 54.4°, 57.1°, and 63.4°, as can be seen in Fig. 2, which is quite similar to that of pure Fe_3O_4 [44], which suggest that almost no change occurs in the structure of Fe_3O_4 after coating by MCM-41 and reveal the inverse cubic spinal structure of iron oxide phrase. The confirming peak showing the presence of molybdate group has appeared in the range of $2\theta = 20°–30°$ which is covered by the broad peak of SiO_2.

Energy-dispersive X-ray analysis (EDX) was used for the structural characterization of Fe_3O_4@MCM-41-$(CH_2)_3$-$OMoO_3H$. As can be seen in Fig. 3, the components of this catalyst include C, O, Fe, Si, and Mo, which indicate the acceptable concordance with the expectations and also confirm the successful incorporation of molybdate groups.

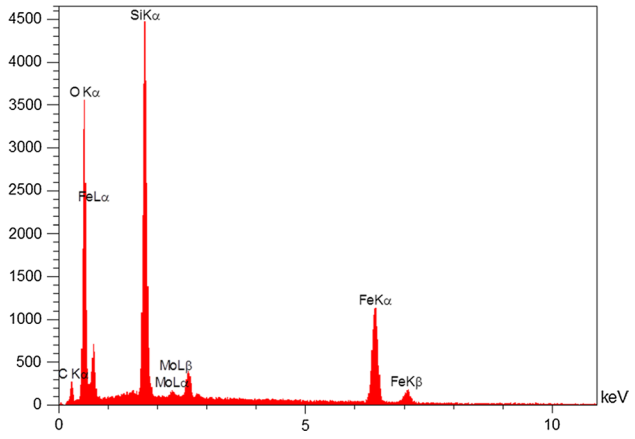

Fig. 3 Energy-dispersive X-ray analysis (EDX) of Fe_3O_4@MCM-41-$(CH_2)_3$-$OMoO_3H$

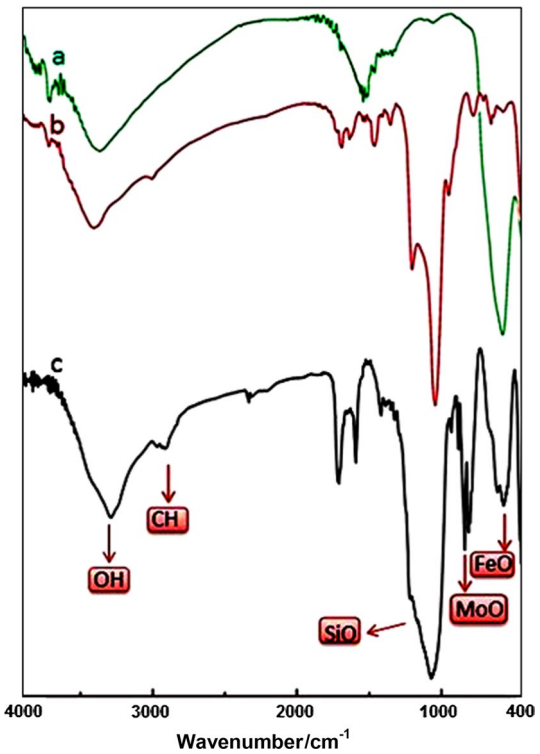

Fig. 4 FT-IR spectra of (a) Fe_3O_4 MNPs, (b) MCM-41, and (c) Fe_3O_4@MCM-41-$(CH_2)_3$-$OMoO_3H$

The FT-IR spectra of Fe_3O_4 MNPs, MCM-41, and prepared Fe_3O_4@MCM-41-$(CH_2)_3$-$OMoO_3H$ are shown in Fig. 4. A broad peak of the OH group was located at about 3305 cm^{-1}. The bands near 589 cm^{-1} and 1085 cm^{-1} can be attributed to the stretching vibration of Fe–O and asymmetric stretching vibration of Si–O–Si, respectively. It can be concluded from the FT-IR pattern of Fe_3O_4@MCM-41-$(CH_2)_3$-$OMoO_3H$ that Fe_3O_4 is coated with MCM-41,

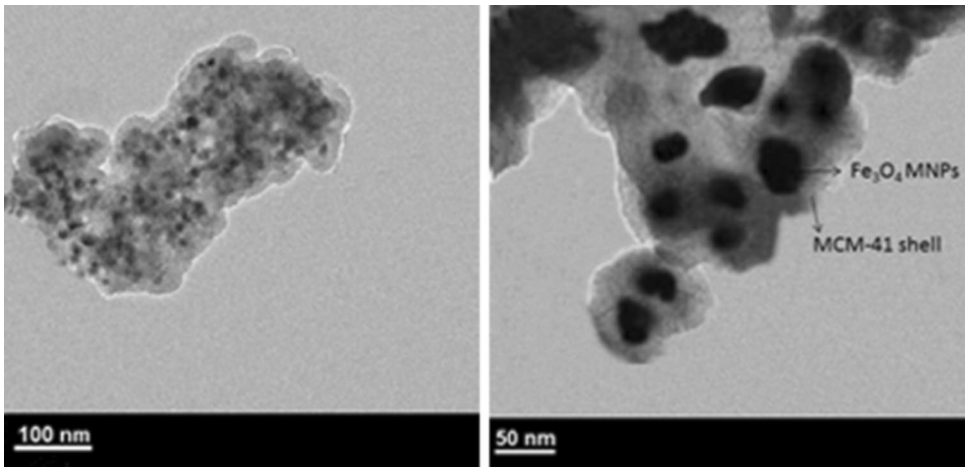

Fig. 5 TEM images of Fe_3O_4@MCM-41-$(CH_2)_3$-$OMoO_3H$

Scheme 2

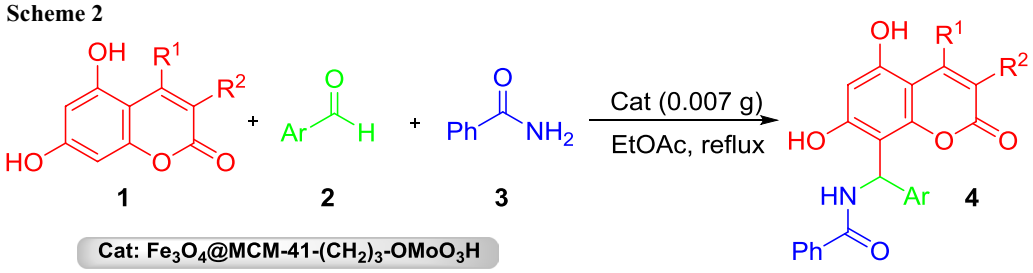

because all the characteristic bands of Fe_3O_4 as well as MCM-41 are found in the spectrum of the catalyst. On the other hand, the band observed at 2930 cm^{-1} may be assigned to stretching vibration of a C–H band. Furthermore, the presence of molybdic acid is confirmed by the band at 995 cm^{-1}, which is related to the stretching vibration of an Mo–O band.

Figure 5 shows the representative TEM images of the Fe_3O_4@MCM-41-$(CH_2)_3$-$OMoO_3H$ nanocatalyst. As can be seen, most of the catalyst is nearly spherical, so that dark magnetic nanoparticle core is surrounded by a lighter MCM-41. Based on TEM images, the particle diameter is about 80–120 nm with almost uniform distribution of magnetic nano particles.

After full characterization of the catalyst, it has been successfully applied to the synthesis of coumarin derivatives **4** by the three-component reaction of 5,7-dihydroxycoumarin derivatives **1**, aryl aldehydes **2**, and benzamide (**3**) (Scheme 2).

The reaction efficiency was highly dependent on the different parameters including the amount of catalyst, solvent, and reaction temperature. Therefore, to get the best experimental conditions, we investigated the model reaction of equimolar quantities of benzamide, benzaldehyde, and 5,7-dihydroxy-4-methylcoumarin. The reaction in the absence of the catalyst was inefficient, and only about 2–5% conversion was obtained even after a long time. Then, we attempted with different amounts of Fe_3O_4@MCM-41-$(CH_2)_3$-$OMoO_3H$ as a catalyst under various conditions. Considering the obtained results, the desired reaction took place efficiently using 0.007 g of the catalyst in ethyl acetate under reflux conditions (Table 1, entry 11). After establishing the optimal conditions, to evaluate the generality and versatility of the introduced procedure, the reaction was loaded with a wide range of aromatic

Table 1 Optimization of the model reaction

Entry	Catalyst/mg	Solvent	Temp./°C	Time/min	Yield/%[a]
1	0	None	25	360	0
2	0	None	50	360	2
3	0	None	90	360	5
4	3	None	90	120	35
5	5	None	90	120	38
6	7	None	90	120	50
7	9	None	90	120	50
8	7	H_2O	Reflux	120	40
9	7	EtOH	Reflux	120	50
10	7	MeOH	Reflux	120	50
11	7	EtOAc	Reflux	60	90
12	7	$CHCl_3$	Reflux	120	60
13	7	EtOAc	25	120	30
14	7	EtOAc	50	120	40

[a]Isolated yields

Table 2 Synthesis of substituted coumarins **4** using Fe_3O_4@MCM-41-$(CH_2)_3$-$OMoO_3H$ (Scheme 2)

Product	R^1	R^2	Ar	Time/min	Yield/%[a]	M.p./°C [References]
4a	$-CH_3$	–H	Ph	60	90	260–261 [45]
4b	$-CH_3$	–H	4-CH_3–Ph	70	80	255–256 [45]
4c	$-CH_3$	–H	3-F–Ph	65	88	268–269 [45]
4d	$-CH_3$	–H	2-HO–Ph	72	77	297–298 [45]
4e	$-CH_3$	–H	2-Cl–Ph	60	85	210–211 [45]
4f	$-(CH_2)_3-$		2-Cl–Ph	65	83	230–231 [45]
4g	$-(CH_2)_3-$		Ph	60	85	270–271 [45]
4h	$-(CH_2)_3-$		2-Br–Ph	80	81	255–256 [45]
4i	$-(CH_2)_3-$		3-F–Ph	60	90	226–227 [45]
4j	$-(CH_2)_3-$		4-F–Ph	65	92	243–244 [45]

[a]Isolated yields

Scheme 3

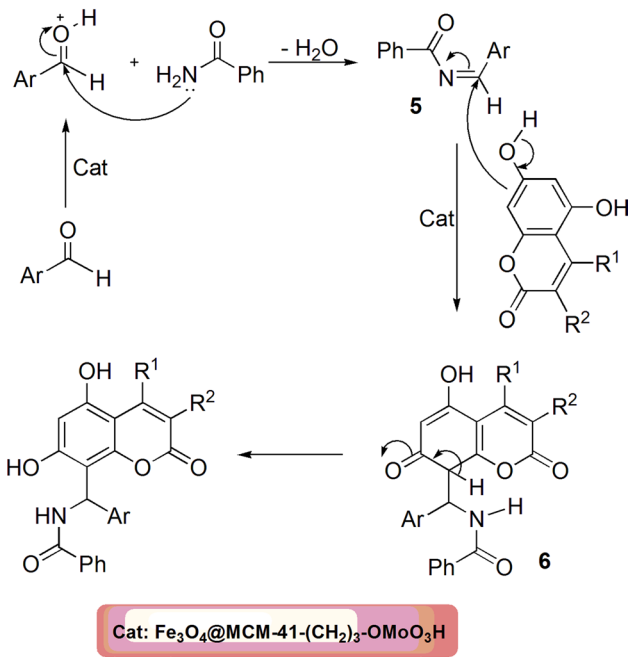

aldehydes and 5,7-dihydroxycoumarins. As shown in Table 2, in all cases, the corresponding products were obtained in good-to-excellent yields.

The proposed mechanism of formation of the product **4** is given in Scheme 3. First, the reaction occurs between benzamide and aryl aldehyde to afford the adduct **5**. Here, it is thought that the acid nanocatalyst can activate the carbonyl group of aldehyde and accelerate the condensation reaction. It is reasonable to assume that, in the presence of nanocatalyst, the adduct **5** to be attacked by C-8 of substituted coumarin which rearranges into product **4**. It should be noted that the existing steric effect at C-6 causes the hydroxyl groups at the C-5 and C-7 positions directly are attack by positions C-8, so the reaction is regioselective [45].

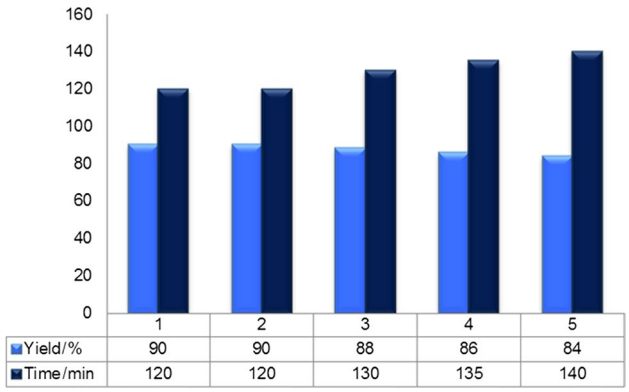

Fig. 6 Reusability of Fe_3O_4@MCM-41-$(CH_2)_3$-$OMoO_3H$ in the reaction of benzamide, benzaldehyde, and 5,7-dihydroxy-4-methylcoumarin

Fe_3O_4@MCM-41-$(CH_2)_3$-$OMoO_3H$ for the one-pot, three-component reaction of benzamide, benzaldehyde, and 5,7-dihydroxy-4-methylcoumarin was checked by separating the catalyst, washing it with MeOH and drying it at 110 °C. As outlined in Fig. 6, the catalyst exhibited no considerable decrease in activity after five cycles.

To test the stability of the catalyst structure, the recycled nanocatalyst was examined by XRD analysis. The diffraction patterns and relative intensities of all peaks matched well to those of the primary catalyst (Fig. 7).

Conclusion

In this research, Fe_3O_4@MCM-41-$(CH_2)_3$-$OMoO_3H$ as a novel nanocatalyst was introduced and characterized by FT-IR, XRD, SEM, EDS, and vibrating sample magnetometer (VSM) analysis. This nanocatalyst demonstrated extremely high reactivity in the environmentally friendly synthesis of coumarin derivatives in high yield and purity. This series of coumarins were designed by the reaction of

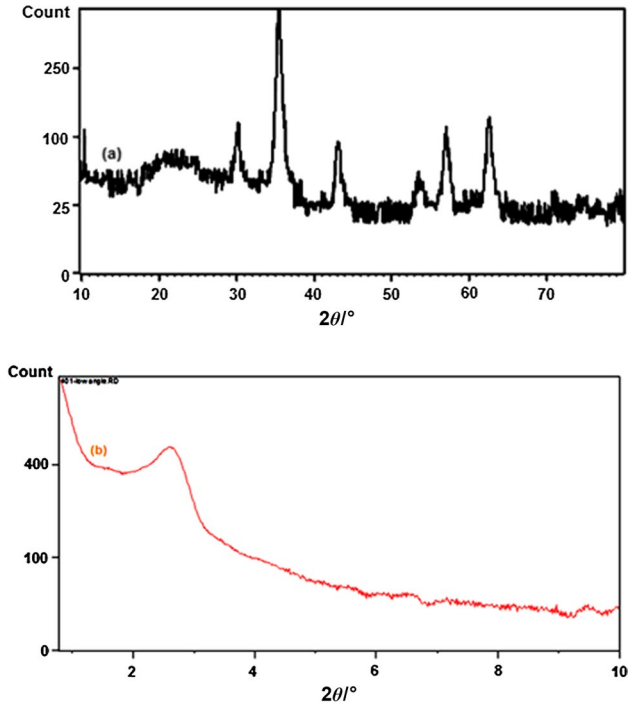

Fig. 7 (a) Wide angle and (b) low angle XRD patterns of recycled catalyst

aryl aldehydes, benzamide, and 5,7-dihydroxycoumarin derivatives. The catalyst can be recovered and reused several times with no decrease in activity.

Experimental

All chemicals used in this research were purchased from Fluka and Merck chemical companies. The obtained products were identified by comparing their spectral data and physical properties with their reported data in the references. The monitoring of the reaction progress and the purity of the compounds were accomplished using TLC performed with silica gel SIL G/UV254 plates. Melting points were determined by an electrothermal KSB1N apparatus. ^{1}H NMR spectra were recorded in DMSO-d_6 on a Bruker Avance UltraShield 400 MHz instrument spectrometers and ^{13}C NMR spectra were recorded at 100 MHz. IR spectra were obtained with a JASCO FT-IR/680 instrument spectrometer using KBr pellets. X-ray powder diffraction (XRD) patterns were recorded using a Bruker AXS (D8 Advance) X-ray diffractometer with Cu Kα radiation ($\lambda = 0.15418$ nm). The measurement was made in 2θ ranging from 10° to 80° at the speed of 0.05° min^{-1}. X-ray spectroscopy (EDX) was obtained using TESCAN vega model instrument. Transmission electron microscopy (TEM) analysis was performed on a JEM 3010 electron microscope (JEOL, Japan) with an accelerating voltage of 300 kV.

Procedure for the preparation of Fe_3O_4 MNPs

For the synthesis of Fe_3O_4 MNPs, 2.5 g $FeCl_2{\cdot}4H_2O$ and 5 g $FeCl_3{\cdot}6H_2O$ (dissolved in 50 cm^3 of distilled water) were added to 6 cm^3 concentrated HCl (12 M), degassed with nitrogen gas, heated to 80 °C, and stirred for 10 min. Then, 10 cm^3 NaOH solution (1.5 M) was added dropwise to the mixture until the brown color solution turned out to be black. The magnetite precipitate (Fe_3O_4 NPs) was separated by an external magnet and washed using double distilled water and ethanol until the pH < 7.5 [46].

Procedure for the synthesis of MCM-41

According to the current method in the literature [47], 4 g cetyltrimethylammonium bromide (CTAB) was dissolved in 1250 cm^3 ammonium hydroxide (1.1 M). Then, 20 cm^3 tetraethoxysilan (TEOS) was added to the prepared solution under vigorous stirring for 30 min. The resulting precipitate was filtered and washed with distilled water, and dried at room temperature and calcinated at 560 °C for 48 h [48].

Preparation of Fe_3O_4@MCM-41-$(CH_2)_3Cl$

MNPs-Fe_3O_4 (2.0 g) was dispersed to a mixture of ethanol and distilled water (70:10 cm^3) by sonication. Then, 5 cm^3 aqueous ammonia (25 wt%) and 1.72 g MCM-41 were slowly added under vigorous stirring at ambient temperature for 24 h. The prepared Fe_3O_4@MCM-41 was separated and washed with ethanol and distilled water and dried at 80 °C. In the next step, in a round-bottomed flask equipped with a condenser and a magnetic stirrer, 3.0 g Fe_3O_4@MCM-41 and 1.5 g (3-chloropropyl)triethoxysilan was suspended in 40 cm^3 dry toluene at 100 °C under N_2 atmosphere and stirred for 24 h. Then, the obtained Fe_3O_4@MCM-41-$(CH_2)_3Cl$ was collected by an external magnet and washed with CH_2Cl_2 and dried in an oven at 50 °C [49].

Preparation of Fe_3O_4@MCM-41-$(CH_2)_3$-$OMoO_3H$

In the final step, Fe_3O_4@MCM-41-$(CH_2)_3$-$OMoO_3H$ was prepared according to the following procedure. A flask was charged with 0.80 g Fe_3O_4@MCM-41-$(CH_2)_3Cl$ and dispersed in 40 cm^3 DMSO in an ultrasonic bath for 30 min. Then, 1.08 g dehydrated sodium molybdate salt was added to the mixture, degassed and stirred under reflux condition. After 24 h, the reaction mixture was collected and washed with DMSO and distilled water and dried. Finally, the brown

precipitate was stirred in the presence of 40 cm^3 HCl (0.1 N) for 5 h. The obtained nanocatalyst was separated by a normal magnet and washed with distilled water and dried overnight under vacuum at 80 °C.

General procedure for the synthesis of coumarins 4

Fe_3O_4@MCM-41-$(CH_2)_3$-$OMoO_3H$ (0.007 g) was added to a mixture of 5,7-dihydroxycoumarins (1 mmol), aryl aldehyde (1 mmol), and benzamide (1 mmol) in 5 cm^3 ethyl acetate and the mixture was stirred under reflux for the requisite time. After completion of the reaction, the catalyst was collected easily by an external magnet and the solvent was removed. Further purification was achieved by recrystallization from ethanol.

Method for the recovery of the catalyst

Fe_3O_4@MCM-41-$(CH_2)_3$-$OMoO_3H$ (0.007 g) was added to a stirred solution of 5,7-dihydroxy-4-methylcoumarin (1 mmol), benzaldehyde (1 mmol), and benzamide (1 mmol) in 5 cm^3 refluxing ethyl acetate. After completion of the reaction, the catalyst was separated by an external magnet and washed with methanol, dried, and reused in subsequent runs.

Acknowledgements The authors gratefully acknowledge the partial support of this work by Yasouj University, Iran.

References

1. Abdollahi Alibeik M, Rezaeipoor Anari A (2016) J Magn Magn Mater 398:205
2. Xie W, Zang X (2016) Food Chem 194:1283
3. Lee CH, Cheng SH, Wang YJ, Chen YC, Chen NT, Souris J, Chen CT, Mou CY, Yang CS, Lo LW (2009) Adv Funct Mater 19:215
4. Chen W, Li X, Pan Z, Ma S, Li L (2016) Chem Eng J 304:594
5. Liu JF, Zhao ZS, Jiang GB (2008) Environ Sci Technol 42:6949
6. Fan G, Wang Y, Yan J, Song G, Li J (2017) J CO2 Util 18:370
7. Sakate S, Kamble S, Chikate R, Rode C (2017) New J Chem 41:4943
8. Liu Y, Li X, Le X, Zhang W, Gu H, Xue R, Ma J (2015) New J Chem 39:4519
9. Girija D, BhojyaNaik H, Vinay Kumar B, Sudhamani C (2011) Am Chem Sci J 1:97
10. Liu Y, Wu N, Wang Z, Cao H, Liu J (2017) New J Chem 41:6241
11. Ge J, Zhang Q, Zhang T, Yin Y (2008) Angew Chem Int Ed 47:8924
12. Zolfigol MA, Ayazi-Nasrabadi R (2016) RSC Adv 6:69595
13. Hudson R, Feng Y, Varma RS, Moores A (2014) Green Chem 16:4493
14. Govan J, Gun'ko YK (2014) Nanomaterials 4:222
15. Rosenholm JM, Zhang J, Sun W, Gu H (2011) Microporous Mesoporous Mater 145:14
16. Ai Y, Hu Z, Shao Z, Qi L, Liu L, Zhou J, Sun H, Liang Q (2018) Nano Res 11:287
17. Liu L, Ai Y, Li D, Qi L, Zhou J, Tang Z, Shao Z, Liang Q, Sun H (2017) ChemCatChem 9:3131
18. Zhou Z, Li Y, Sun H, Tang Z, Qi L, Liu L, Ai Y, Li S, Shao Z, Liang Q (2017) Green Chem 19:3400
19. Kefayati H, Kohankar AM, Ramzanzadeh N, Shariati S, Bazargard SJ (2015) J Mol Liq 209:617
20. Li Y, Duan D, Wu M, Li J, Yan Z, Wang W, Zi G, Wang J (2016) Chem Eng J 306:777
21. Kowalczyk A, Borcuch A, Michalik M, Rutkowska M, Gil B, Sojka Z, Indyka P, Chmielarz L (2017) Microporous Mesoporous Mater 240:9
22. Safari J, Zarnegar Z (2015) RSC Adv 5:17738
23. Ali Z, Tian L, Zhang B, Ali N, Khan M, Zhang Q (2017) New J Chem 41:8222
24. Abrokwah RY, Deshmane VG, Kuila D (2016) J Mol Catal A Chem 425:10
25. Khorshidi A, Shariati S (2014) RSC Adv 4:41469
26. Saadatjoo N, Golshekan M, Shariati S, Kefayati H, Azizi P (2013) J Mol Catal A Chem 377:173
27. Jha A, Patil CR, Garade AC, Rode CV (2013) Ind Eng Chem Res 52:9803
28. Hu YQ, Xu Z, Zhang S, Wu X, Ding JW, Lv ZS, Feng LS (2017) Eur J Med Chem 136:122
29. Kulkarni M, Kulkarni G, Lin C, Sun C (2006) Curr Med Chem 13:2795
30. Sánchez-de-Armas R, San Miguel MÁ, Oviedo J, Sanz JF (2012) Phys Chem Chem Phys 14:225
31. Lunazzi L, Mancinelli M, Mazzanti A, Pierini M (2010) J Org Chem 75:5927
32. Arshad A, Osman H, Bagley MC, Lam CK, Mohamad S, Zahariluddin ASM (2011) Eur J Med Chem 46:3788
33. Zhou S, Jia J, Gao J, Han L, Li Y, Sheng W (2010) Dyes Pigments 86:123
34. Pang GX, Niu C, Mamat N, Aisa HA (2017) Bioorg Med Chem Lett 27:2674
35. Sripathi S, Logeeswari K (2013) Int J Org Chem 3:42
36. Valizadeh H, Shockravi A (2005) Tetrahedron Lett 46:3501
37. Olomola TO, Klein R, Lobb KA, Sayed Y, Kaye PT (2010) Tetrahedron Lett 51:6325
38. Farahi M, Karami B, Tanuraghaj HM (2015) Tetrahedron Lett 56:1833
39. Patil PO, Bari SB, Firke SD, Deshmukh PK, Donda ST, Patil DA (2013) Bioorg Med Chem Lett 21:2434
40. Farahi M, Karami B, Banaki Z, Rastgoo F, Eskandari K (2017) Monatsh Chem 148:1469
41. Farahi M, Davoodi M, Tahmasebi M (2016) Tetrahedron Lett 57:1582
42. Farahi M, Tamaddon F, Karami B, Pasdar S (2015) Tetrahedron Lett 56:1887
43. Behbahani M, Ali Akbari A, Amini MM, Bagheri A (2014) Anal Methods 6:8785
44. Sharma RK, Dutta S, Sharma S, Zboril R, Varma RS, Gawande MB (2016) Green Chem 18:3184
45. Karami B, Farahi M, Farmani N, Tanuraghaj H (2016) New J Chem 40:1715
46. Wu ZS, Yang S, Sun Y, Parvez K, Feng X, Müllen K (2012) J Am Chem Soc 134:9082
47. Wang Y, Yu Y, Deng C, Wang J, Zhang BT (2015) RSC Adv 5:103989
48. Shao Y, Jing T, Tian J, Zheng Y (2015) RSC Adv 5:103943
49. Elmekawy AA, Sweeney JB, Brown DR (2015) Catal Sci Technol 5:690